AUSTRALIAN JOURNAL OF MECHANICAL ENGINEERING
https://doi.org/10.1080/14484846.2021.1958992

Taylor & Francis
Taylor & Francis Group

ARTICLE

Effect of contact geometry on temperature field distribution and thermal buckling of an in-wheel disc brake system

Kingsford Koranteng, Joseph-Shaahu Shaahu and Yun-Bo Yi

Department of Mechanical and Materials Engineering, University of Denver, Denver, USA

ABSTRACT

This paper aims to determine the effect of contact geometry on temperature distribution and thermal buckling in an in-wheel brake system. Numerical analysis is conducted to investigate the variation of temperature field distribution on the brake disc a different cover angles of the pad while maintaining the same moment of friction. Also, different positions of the pads on the disc are considered. To verify the simulation results, an analytical solution is derived. The results show that, for the same work done by the pads on the disc, the resulting temperature field distributions have various effects on the disc. Moreover, certain contact geometry was found to cause the braking temperature to exceed the critical temperature, leading to thermal buckling of the disc during braking.

ARTICLE HISTORY
Received 12 March 2021
Accepted 19 July 2021

KEYWORDS
Temperature; pad cover angle; thermal buckling; in-wheel mounted brake

1. Introduction

The demands and research on in-wheel motor-driven vehicles for both hybrid and fully electric vehicles have increased steadily over the past years due to the numerous advantages provided by this technology (Hwang et al., 2008). The technology is very useful in the application of military vehicles with wheels speed and steering control being independent of each other since each wheel is driven by a separate electric motor. This has the potential of creating an all-wheel-drive system for the vehicle. More importantly, it makes it easier to develop a simple intelligent brake system with an appropriate control strategy for the anti-lock brake system (Choi and Lee 2004). Besides, because the hydraulic brake components are mounted within the wheels, the brake system is referred to as an in-wheel brake system. Figure 1 shows the schematic of a 10 × 10 hybrid vehicle with an in-wheel motor-driven system. The power is either provided by the internal combustion engine or the energy stored in the battery. Further, each wheel has an electric motor attached to provide rotational motion utilising a set of planetary gears. Two main types of braking take place within each of the wheels. These are electrical braking (regenerative braking) and hydraulic braking. The hydraulic brake serves as a backup whenever there are electrical glitches and also during steep deceleration at full vehicle load.

This paper focuses on the hydraulic braking components mounted within the wheel. A major challenge with this technology is the design of the disc brake components, which are usually mounted within the wheels. The available space within each wheel for the design of an appropriate disc brake system is limited, even in the case of heavy vehicles. Moreover, the enclosed nature of the brake system contributes to poor heat dissipation, which may lead to the early onset of thermal buckling and thermoelastic instability during braking. The in-wheel brake system comprises a steel rotor disc that can move axially, a fixed brake pad, an actuation system, and at least one axially moving brake pad provided on each side of the rotor disc as shown in (Figure 2). Moreover, when the fixed and the axial moving pad clamp against the disc, frictional heat is produced. The resulting heat generation maybe somewhat high due to poor natural convection, which leads to several negative effects such as thermal buckling, thermal cracks, thermal hot spot, brake fade, and also damage to the attached electric motors (Hwang, Wu, and Jeon 2008; Choi and Lee 2004; Grzes et al. 2016; Ghadimi, Sajedi, and Kowsary 2013). The aforementioned effects are a result of non-uniform temperature distribution on the brake disc during sliding interaction between the pad and disc (Karan Dhir 2018; Belhocine and Bouchetara 2012). This phenomenon has been found to promote thermal buckling, which in turn promotes thermoelastic instability (Chen et al. 2019; Yi, Shaahu, and Chen 2018; Koranteng et al. 2020; Shaahu, Koranteng, and Yi 2020). The coupling between thermoelastic instability and thermal bucking was investigated by Chen et al. (Chen et al. 2019). These authors found that unstable temperature modes induced by thermoelastic instability can influence the temperature profiles for thermal buckling. In addition, the same author developed a finite element model to detect thermal buckling

CONTACT Kingsford Koranteng Kingsford.koranteng@du.edu

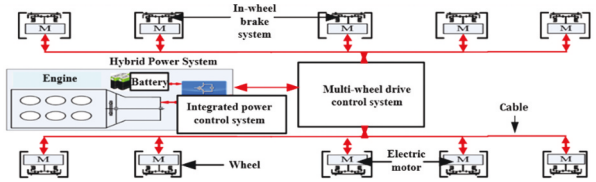

Figure 1. Schematics of an in-wheel motor-driven hybrid vehicle.

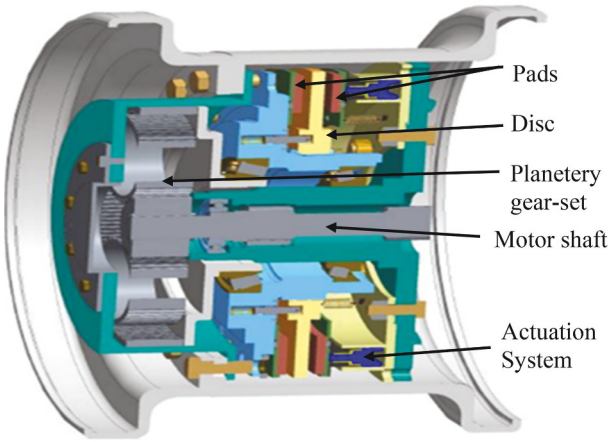

Figure 2. Structure of the in-wheel brake system.

in sliding systems (Chen, Yi, and Zhao 2016). They discovered that there is a specific wavenumber with which the buckling temperature approaches a minimum value. In brake design, especially in the case of in-wheel brake systems, it is necessary to predict the temperature field distribution and the corresponding buckling mode during the design stages to prevent uncertainty in brake performance (Vescovini and Dozio 2018).

In this paper, a disc brake system designed for a 10 × 10 multi-in-wheeled motor-driven vehicle is studied during braking at full vehicle load. The vehicle travels in a straight path without steering on a flat road using TRUCKSIM. The resulting dynamic force distributions on each wheel during the braking period are obtained. Besides, the ultimate objective of this work and a major difference between this and prior research work is that this work considers a special case of a disc brake system designed to be mounted within the wheels of a hybrid vehicle by investigating the influence of different cover angles of the pad and its positions on temperature field distributions. Further, the effect of the radial temperature field distribution on thermal buckling is studied using a linear perturbation approach.

At present, there are few works on the brake system of an in-wheeled vehicle that considers the vehicle dynamic forces during braking , the effect of contact geometry on temperature field distribution and thermal buckling. The current study uses a dynamic temperature-displacement

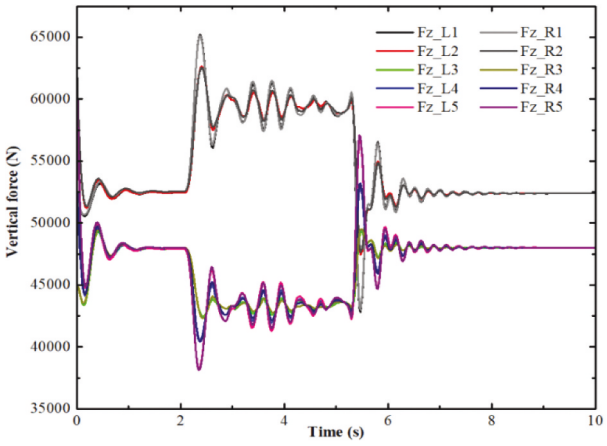

Figure 3. Vertical load acting on each wheel of the vehicle.

and buckling analysis to investigate these phenomena and the results are discussed.

2. Thermal analysis of the disk rotor and pad contact

In order to begin the thermal analysis, the reference 10 × 10 vehicle weight distributions on the individual wheels at full load (5000 kg) are studied using TRUCKSIM. The resulting dynamic vertical force $F_{z\ (L,\ R)\ m}$distribution on the individual wheels during braking at t = 2.0s with a speed of 30 km/h is shown in (Figure 3). For analysis purposes, we considered one of the front wheels of the reference vehicle for this study. From the resulting forces in (Figure 3), we computed the ratio of the weight distribution on the front wheels to be approximately 0.59. Further, the required parameters needed to carry out the numerical studies were also computed. The influence of contact geometry and the resulting temperature field effect on thermal buckling is investigated.

3. Analytical approach

We considered the reference vehicle to be moving in a straight path with an initial velocity of 30 km/h. The energy of the vehicle during deceleration from the initial velocity to a final destination can be expressed in Eq. (1).

$$E_b = \frac{1}{2}\left[M(v_i^2 - v_f^2) + I(\omega_i^2 - \omega_f^2)\right] \tag{1}$$

Further, if the vehicle comes to a complete stop, the final velocity and angular velocity becomes zero and Eq. (1) becomes:

$$E_B = \frac{1}{2}\left[M(v_i^2) + I(\omega_i^2)\right] \tag{2}$$

Moreover, when the vehicle is at a complete stop, the decelerating power of the brakes can be obtained by

finding the derivative of the vehicle kinetic energy during the braking time as expressed in Eq. (3).

$$P_d = \frac{d}{dt}\left(\frac{Mv^2}{2}\right) = Mv\frac{dv}{dt} = MR^2\omega(t)\alpha_t \tag{3}$$

Where $\omega(t)=\omega_0+\alpha_t t$

Also, α_t represents the angular acceleration of the vehicle. We assumed that the brake decelerating power is equivalent to the total friction heat source during braking.

$$P_d = P_f$$

Moreover, since each wheel of the reference 10 × 10 vehicle has four brake pads mounted within, there will be a total of 40 brake pads. Therefore, the friction heat generated can be expressed by the integral below:

$$P_f = 40\int (f_f.v)dAp = (-40)f_f(t)\int rdAp \tag{4}$$

Equations 3 and 4 can be combined to obtain the total friction force f_f generated by the vehicle during braking [13]:

$$f_f = \frac{MR^2\alpha_t}{40r_mAp} \tag{5}$$

From Eq. (5), the total heat generated by the vehicle is obtained by finding the dot product of the vehicle velocity and the friction force.

$$q(r,t) = \gamma.f_f.v(t) = \gamma\left(\frac{mR^2\alpha_t}{40r_mAp}.r(\omega_o+\alpha_t t)\right) \tag{6}$$

Also, by considering the following conditions:

Weight distribution on the front wheel = 0.59;

Only one front brake rotor is considered = 1/4;

Only one side of the rotor is considered = 0.5.

The heat flux on one side of a single rotor for a single front wheel can be computed as:

$$\begin{aligned} q(r,t) &= \dot{Q}_{in} = \gamma.f_f.v(t) \\ &= (0.59)\frac{1}{4}(0.5)\gamma\left(\frac{mR^2\alpha_t}{40r_eA_p}r(\omega_o+\alpha_t t)\right) \end{aligned} \tag{7}$$

In addition, the equilibrium equation for the heat generated can be expressed as:

$$\begin{aligned} C_p.m_d.\frac{dT}{dt} &= \dot{Q}_{in}(Q_{brake\_heat}) \\ &\quad - \dot{Q}_{out}(Q_{conduction}+Q_{convection}) \end{aligned} \tag{8}$$

$$C_pm_d\frac{dT}{dt} = \dot{Q}_{in} - K_dAd(T_s-T_a) - hA_s(T_s-T_a) \tag{9}$$

Equation 7 can be substituted into Eq. 9 to obtain an expression for the change in temperature within the disc during braking as expressed in Eq. 10. From this expression, a Simulink model was developed to compute the temperature change during braking.

$$\begin{aligned} \frac{dT}{dt} = &-\frac{K_dA_dT_s}{C_pm_d} - \frac{hA_sT_s}{C_pm_d} + \\ &\frac{(0.59)\frac{1}{4}(0.5)\gamma\left(\frac{MR^2\alpha_t}{40r_eAp}r(\omega_o+\alpha_t t)\right) + K_dA_dT_a + hA_sT_a}{C_pm_d} \end{aligned} \tag{10}$$

Here, the heat transfer coefficient (h) in Eq. 10 was estimated by first computing Reynold's number using the expression in Eq. 11:

$$\mathrm{Re} = \frac{\omega r^2}{\nu} < 2.4\times10^5 \tag{11}$$

Utilising equation 11, a laminar flow of Reynold's number ($\mathrm{Re}< 2.4\times10^5$) was obtained. The heat transfer coefficient for the disc was then computed using Eq. 12.

$$h = 0.04\left(\frac{K_a}{D}\right)\mathrm{Re}^{0.8} \tag{12}$$

3.1. Numerical modelling

The finite element analysis was carried out by considering only the pad and brake disc due to the high cost of computing the complete structure (Wang and Fu 2013). Moreover, since both the disc and pads are symmetric, only half of the sections were considered, and boundary conditions are defined as shown in (Figure 4). The disc and pad were modelled in ABAQUS using an 8-node thermally coupled brick, trilinear displacement, reduced integration, hourglass control element (C3D8T element) as shown in (Figure 5). The disc and the annular pads have an inner radius:r_d = 112 mm and r_p = 173.5 mm respectively, and outer radius R_d = 232 mm and R_p = 237 mm, respectively. The friction ring section and the pad are 5 mm and 10 mm in thickness, respectively. The radial distance of the friction ring section which is from the outer radius (R_o) of the disc hub to the outer radius of the disc R_d is dx = 90 mm. The simulation was conducted by performing a coupled temperature-displacement analysis with ABAQUS dynamic temp-disp explicit scheme to determine the

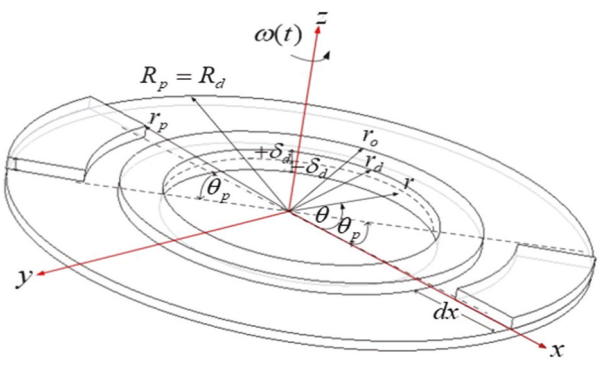

Figure 4. Geometry of the brake disc and pad.

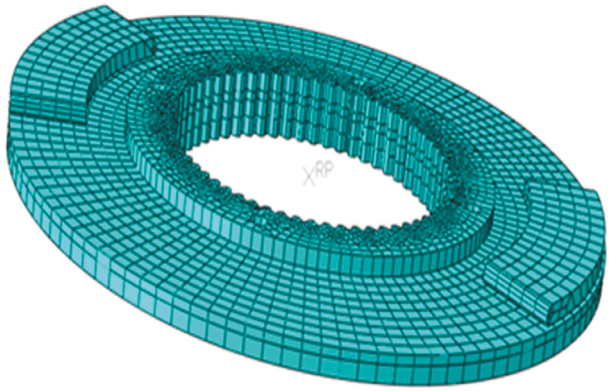

Figure 5. 3-D mesh of the brake disc and pads.

influence of pad cover angle (θ_p) and its positions on the temperature field distribution on the disc by ensuring the same moment of friction irrespective of change in geometry or position. We defined a surface-to-surface interaction between the pad and disc contact area and ignored the effect of radiation during sliding interaction due to the enclosed nature of the in-wheeled mounted brake-disc system. The convection boundary conditions were defined on all free surface areas of the pad and disc. The average convection heat coefficient for the convection boundary conditions was computed to be h = 5 W/m^2/°C. (Tables 1 and 2) show the material properties and parameters used in the simulation process.

Assuming that all friction resulting from the braking process is dissipated as heat, the heat flux generated at the contact interface $Z = 0$ enters the pad and the disc, respectively, according to equations 13 &14.

Table 1. Parameters & thermoelastic properties used in the simulation.

Dimension	Disc (65Mn steel)	Pad
Elastic modulus, $E_{p,d}$ (GPa)	211	100
Poison's ratio, υ	0.288	0.25
Thermal conductivity, K[W/(m^{2}°C)]	48	0.5
Specific heat, $c_{p,d}$ [J/(k°C)]	450	1000
Mass density, $\rho_{p,d}$(Kg/m^3)	7820	1400
Mass of the brake disc m_d,kg	2.0	
Initial Velocity V_o, km/h	30	
Angular velocity $_o$, rad/s	14	
Vehicle mass, Kg	50,000	

Table 2. Dimensions and application parameters of the vehicle braking.

Dimension	**Disc**	**Pad**
Inner radius $r_{p,d}$, m	0.112	0.173
Initial outer radius, $R_{p,d}$, m	0.237	0.232
Hub Outer radius r_o, m	0.147	
Friction ring thickness, $\delta_{p,d}$(m)	0.005	0.010
Thickness δ_d (hub portion)	0.025	
Effective radius, $re_{p,d}$	0.340	0.374
Wheel radius R, m	0.6	20,30,40,50,60,70,80,90,100
Variable parameters		0,1,2,3,4,5,6,7
Pad angle θ_p		
Pad position from the disc circumference (mm)		

$$q_p(r,\theta,0,t) = \gamma f_f p\omega(t) r, r_p \le r \le R_p, 0 \le \theta \le \theta_p, 0 \le t \le t_s \tag{13}$$

$$q_d(r,\theta,0,t) = (1-\gamma) f_f p\omega(t) r, r_p \le r \le R_p, 0 \le \theta \le 2\pi, 0 \le t \le t_s \tag{14}$$

Whereγ is the heat partition ratio (Talati and Jalalifar 2009; Adamowicz and Grześ 2012; Yevtushenko and Grzes 2011)calculated as:

$$\gamma = \frac{K_p\sqrt{\alpha_d}}{K_p\sqrt{\alpha_d} + K_d\sqrt{\alpha_p}} \tag{15}$$

Here, K is the thermal conductivity, α is the thermal diffusivity and the subscripts p and d represent pad and disc, respectively. The governing equations for the three-dimensional temperature fields T (r, θ, z, t) of the pad and disc are presented as follows.

Governing equation for the disc:

$$K_d\left(\frac{\partial^2 T}{\partial r^2} + \frac{1}{r}\frac{\partial T}{\partial r} + \frac{1}{r^2}\frac{\partial^2 T}{\partial \theta^2} + \frac{\partial^2 T}{\partial z^2}\right) = \rho c_p\left[\frac{\partial T}{\partial t} + \frac{V(t)}{R}\frac{\partial T}{\partial \theta}\right], \tag{16}$$

$$r_d < r < R_d, 0 < \theta < 2\pi, -\delta_d < z < 0, t < 0 < t_s$$

,

$$r_d < r < r_o, 0 < \theta < 2\pi, 0 < z < +\delta_d, t < 0 < t_s$$

Governing equation for a single pad:

$$K_p\left(\frac{\partial^2 T}{\partial r^2} + \frac{1}{r}\frac{\partial T}{\partial r} + \frac{1}{r^2}\frac{\partial^2 T}{\partial \theta^2} + \frac{\partial^2 T}{\partial z^2}\right) = \rho c_p\frac{\partial T}{\partial t}, \tag{17}$$

$$r_p \le r \le R_p, 0 \le \theta_p, 0 < z < \delta_p, 0 < t < t_s$$

In the analysis, boundary conditions were applied appropriately to depict the real working condition of the brake system of the vehicle. Initial boundary conditions for the temperature distribution in the disc and pad were taken to be at ambient temperature. These were defined as follows:

$$T(r,\theta,z,0) = T_a, r_p \le r \le R_p, \tag{18}$$

$$T(r,\theta,z,0) = T_a, r_d \le r \le R_d, 0 \le \theta \le 2\pi, -\delta_p \le z \le 0 \tag{19}$$

$$T(r,\theta,z,0) = T_a, r_d \le r \le r_o, 0 \le \theta \le 2\pi, 0 \le z \le +\delta_d \tag{20}$$

In addition, at the contact surface were the pad and the disc interact, the initial boundary condition was expressed as:

$$K_d\frac{\partial T}{\partial z}\bigg|_{z=0^-} - K_p\frac{\partial T}{\partial z}\bigg|_{z=0^+} = q(r,\theta,0,t),\ (r,\theta)\in A_s, 0 \le t \le t_s \tag{21}$$

Further, the temperature at the contact interface between the pad and disc during sliding can be expressed as:

$$T(r,\theta,0^+,t) = T(r,\theta,0^-,t),\ (r,\theta)\in A_d, 0 \le t \le t_s \tag{22}$$

More importantly, to account for heat convection during the braking period, convection boundary conditions were defined at all free surface areas of the pad and disc. The convection boundary conditions for the disc were defined as follows:

$$K_d\frac{\partial T}{\partial r}\bigg|_{r=r_d} = h[T(r_d,\theta,z,t) - T_a],\ 0 \le \theta \le 2\pi, -\delta_d < z < 0, 0 < z < +\delta_d, 0 \le t \le t_s \tag{23}$$

$$K_d\frac{\partial T}{\partial r}\bigg|_{r=R_d} = h[T_a - T(R_d,\theta,z,t)],\ 0 \le \theta \le 2\pi, -\delta_d < z < 0, 0 \le t \le t_s \tag{24}$$

$$K_d\frac{\partial T}{\partial r}\bigg|_{r=r_o} = h[T_a - T(r_o,\theta,z,t)],\ 0 \le \theta \le 2\pi, 0 < z < +\delta_d, 0 \le t \le t_s \tag{25}$$

$$K_d\frac{\partial T}{\partial z}\bigg|_{z=+\delta_d} = h[T_a - T(r,\theta,+\delta_d,t)],\ r_d < r < r_o, 0 \le \theta \le 2\pi, 0 \le t \le t_s \tag{26}$$

$$K_d\frac{\partial T}{\partial z}\bigg|_{z=0^-} = h[T_a - T(r,\theta,0^-,t)],\ r_o < r < r_p, 0 \le \theta \le 2\pi, 0 \le t \le t_s \tag{27}$$

$$K_d\frac{\partial T}{\partial z}\bigg|_{z=0^-} = h[T_a - T(r,\theta,0^-,t)],\ r_p < r < R_p, 0 \le \theta \le 2\pi, 0 \le t \le t_s \tag{28}$$

4. Simulation results

4.1. Influence of pads cover angle on temperature distribution

The discs were labelled S1, S2, S3, S4, S5, S6, S7, S8, and S9 with corresponding pad cover angles θ_p of 20°, 30°, 40°, 50°, 60°, 70°, 80°, 90°, and 100° respectively. These cover angles were selected for the analysis because the reference vehicle requires large braking torque at full load, especially when descending hills and slopes. In normal cars, the cover is approximately 60°, however, in heavy-duty military vehicles and aircraft, the cover angle maybe equal to 360°. Nonetheless, the limited space within the wheels and the quest for optimum weight require a careful selection of the cover angle of the pad. The numerical simulation was carried out using ABAQUS for single braking at time t_s = 4.2 s for the vehicle decelerating with an initial velocity of 30 km/h to standstill.

(Figure 6) illustrates the pad cover angle θ_p which was varied in this work. It is quite clear that increasing the pad cover angles $\theta_p$for each simulation will result in an increased contact area of the pad which in turn increases the force applied on the rotor. This leads to differences in the moment of friction or work done if the process is to be repeated for different pad cover angles. Therefore, it is inaccurate to make a comparison or draw conclusions from the simulation results. Hence, we computed the corresponding applied pressure required for each angle $\theta_p$of the pad to produce the same moment of friction or work done on the disc during the braking period. A similar technique involving a single pad was used by Grześ (Grześ 2014) but did not take into consideration the effect of the resulting temperature field on thermal buckling. (Figure 7) shows the temperature field distribution on the disc for four selected cover angles of the pads. The temperature field distributions on the discs are non-uniform as expected but appeared to have a similar distribution pattern. The red zone of the temperature distribution appeared close to the circumferential region of each disc. This could be attributed to velocity being maximum at the circumferential region and decreasing along the radial direction. In addition, the similarities in the temperature fields on the disc could be attributed to the same friction force generated during sliding contact between the pad and disc. Nevertheless, there were discrepancies in the resulting maximum temperature for each disc. The disc labelled S1 exhibited the highest maximum temperature T_{max} = 355.40°C whereas the disc S9 showed the lowest maximum temperature T_{max} = 355.40°C. In summary, the increasing maximum temperatures of the discs were in the order of decreasing pad cover angles.

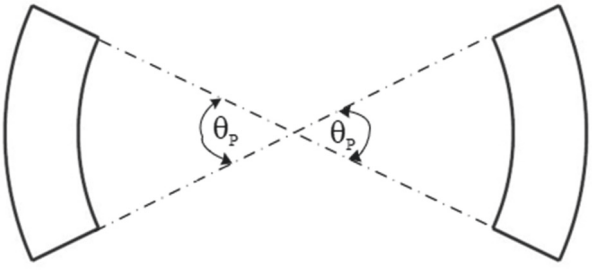

Figure 6. Diagram showing the cover angle of the pad.

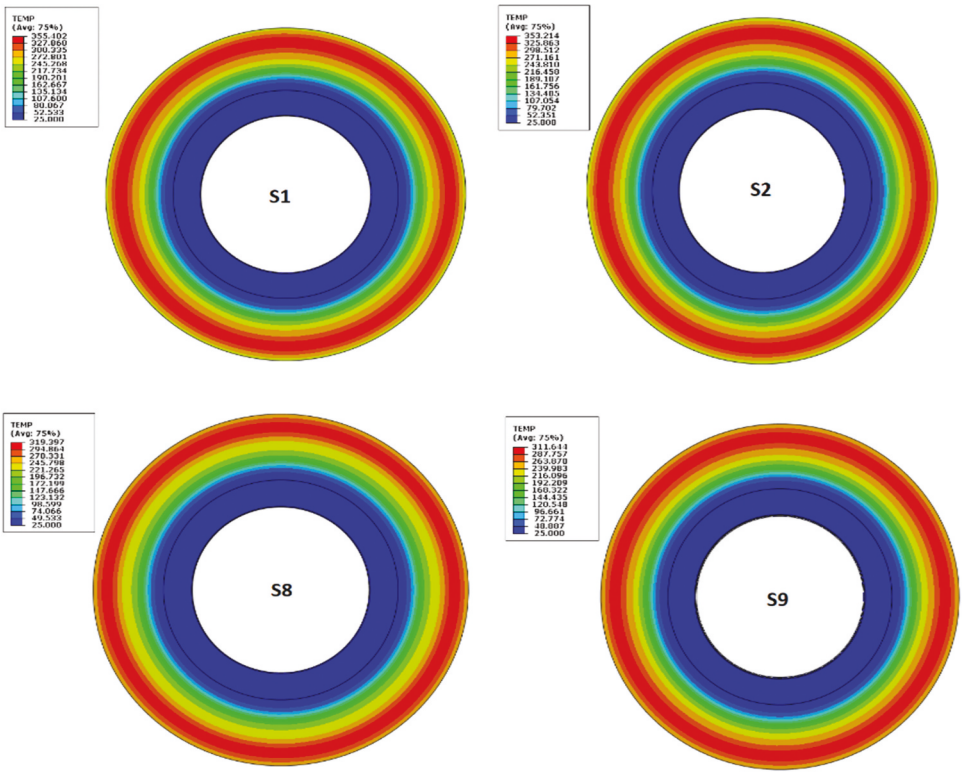

Figure 7. Variation of temperature field on disc for different cover angles of the pads.

Thus, for the same work done, braking with a smaller pad cover angle will lead to a high-temperature distribution at a localised area on the disc. Conversely, a larger pad cover angle leads to a smaller maximum temperature, however, the unsprung mass of the reference vehicle increases.

We validated the simulation by comparing the numerical results with the developed mathematical model from Eq. 10 using MATLAB Simulink. It was found that the numerical and analytical solutions are not well correlated as there were several assumptions made like different heat transfer coefficients, boundary conditions, etc. Besides, the FEA depicts more realistic modelling of the sliding components, material properties and boundary conditions, and also takes into account nonlinearities [29]. Therefore, the expected qualitative and quantitative differences. For example, comparing the analytical and numerical results for braking with the pad cover angle of 30° as shown in (Figure 8), the evolution of temperature for the analytical and the numerical simulation begins at room temperature of 25°C and reached maximum values of 305°C and 353°C, respectively.

More importantly, there exists a great relationship between temperature distribution and the pad cover angle (Figure 9). The temperature profile pattern with time for each disc shows a similar trend, however, the order of increasing value of temperature with time differs from each disc, with the highest being the disc with the smallest pad cover angle.

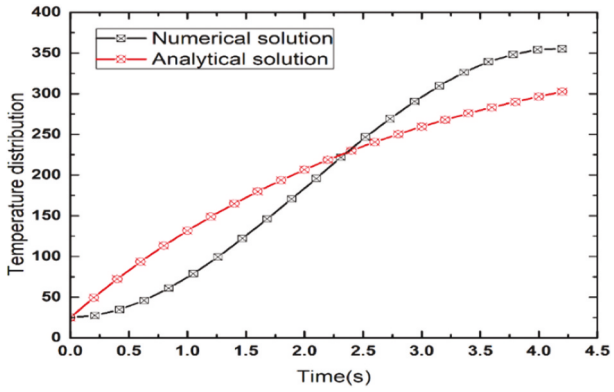

Figure 8. Variation of maximum temperature with time at different cover angles of the pads.

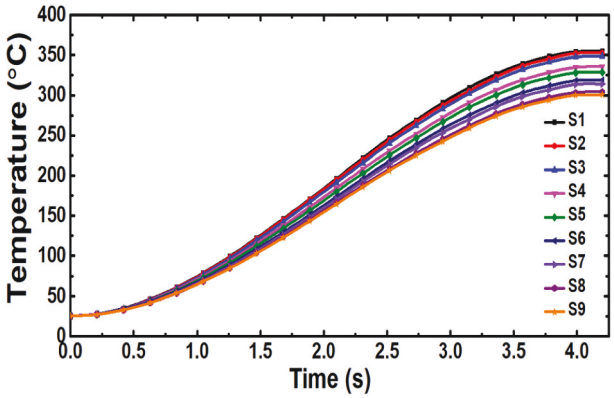

Figure 9. Temperature distribution through the disc rotor at 30° pad cover angles.

Furthermore, because the angular velocity of the rotating disc is always maximum at the earlier stages of the braking process, the temperature is seen to rise faster in all the discs at the early stages and then slows down at the latter stages of braking due to the convection heat transfer defined at the free surface area of the disc. The maximum temperature reach at the stop of the disc indicates that there is equilibrium between the heat flux generated during braking and convection heat loss. The resulting difference in the maximum temperature field distribution from S1 to S9 is attributed to the heat partition ratio. Despite the same heat partition ratio used for the analysis, the resulting friction heat distributions into the disc and pad were slightly different. This is because the heat partition coefficient depends strongly on the geometry of the pads (He and Ovaert 2008). The geometry has a strong relationship with the mutual overlap coefficient (η) during braking, which can be defined as the ratio of the contact area of the pad to the sliding track area. This is given by the equation:

$$\eta = \frac{\theta_p}{2\pi} \tag{29}$$

In practice, the mutual overlap coefficient changes and becomes less than one. Hence, Equation (15) which is mostly used to calculate the heat partition ratio in clutches and brakes when the mutual overlap coefficient is equal to 1 needs to be replaced with Newcomb, 1958 formula (Grze 2011).

$$\gamma = \frac{\eta K_p \sqrt{\alpha_d}}{\eta K_p \sqrt{\alpha_d} + K_d \sqrt{\alpha_p}} \tag{30}$$

From Newcomb's formula, we can see that the cover angle has a great relationship with the mutual overlap coefficient. Therefore, when the mutual overlap coefficient changes, the heat partition ratio is affected slightly which may contribute to the difference in the temperature distribution values on the disc, irrespective of the same friction work done by the pads on the disc.

Further, we investigated the temperature distribution along the radial direction of the friction ring section of the disc at different cover angles of the pads as shown in (Figure 10). The radial temperature profile on the disc for each varied cover angle of the pad exhibited the same trend. The maximum temperature on the disc occurred at the same radial distance (dx = 71.0 mm). This is expected because the friction work is the same. Nonetheless, the peak temperature distribution values were found to be different. This behaviour forms an important part of this work because it can lead to thermal buckling of the disc as investigated in Section 4.3.

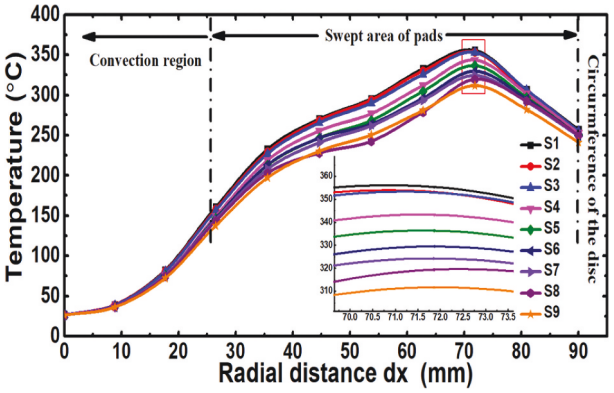

Figure 10. Distribution of temperature along the radial of the disc for different cover angles of the pads.

4.2. *Influence of pads position on temperature distribution*

The discs were labelled P1, P2, P3, P4, P5, P6, P7 and P8 with corresponding pads positioned at $R_p = R_d$, (r_p = 172.13 < r < R_p = 236) mm, (r_p = 170.76 < r < R_p = 235) mm, (r_p = 169.38 < r < R_p = 234) mm, (r_p = 168 < r < R_p = 233) mm, (r_p = 166.61 < r < R_p = 232) mm, (r_p = 165.21 < r < R_p = 231) mm, (r_p = 163.81 < r < R_p = 230) mm respectively. More precisely, the outer radius of the pads is positioned at 0 mm,1 mm, 2 mm,3mm,4 mm,5 mm,6mm, and 7 mm away from the circumference of the disc, respectively. This was done to investigate the influence of pad positions on the temperature distribution in the brake disc. In the simulation, the inner and outer radius of the pads were altered such that they provided the exact aforementioned positions on the disc rotor while maintaining the same contact area. Interestingly, at different positions on the disc, the resulting braking torque will be different. Therefore, in order to maintain the friction work by each pad on the disc, we computed the braking time and torque required to generate the same friction force on each disc during braking. The resulting temperature field distribution on the discs from P1 to P8 is observed as shown in (Figure 11). The temperature field distributions on the disc were highly non-uniform as expected. The temperature field distribution for P1, P2, P3, and P4 showed a similar distribution pattern but with different magnitudes during the braking period. The deep red zone appeared to have a more spread area compared to the light red zone. This observation is because, at these positions, the temperature distribution is influenced by the sliding velocity compared to convection losses on the free surfaces of the disc.

Meanwhile, at P5, P6, and P7, the light red zone appeared to have the same radial distance as the deep red zone on the disc. This behaviour can be attributed to the radial reduction in sliding velocity at these

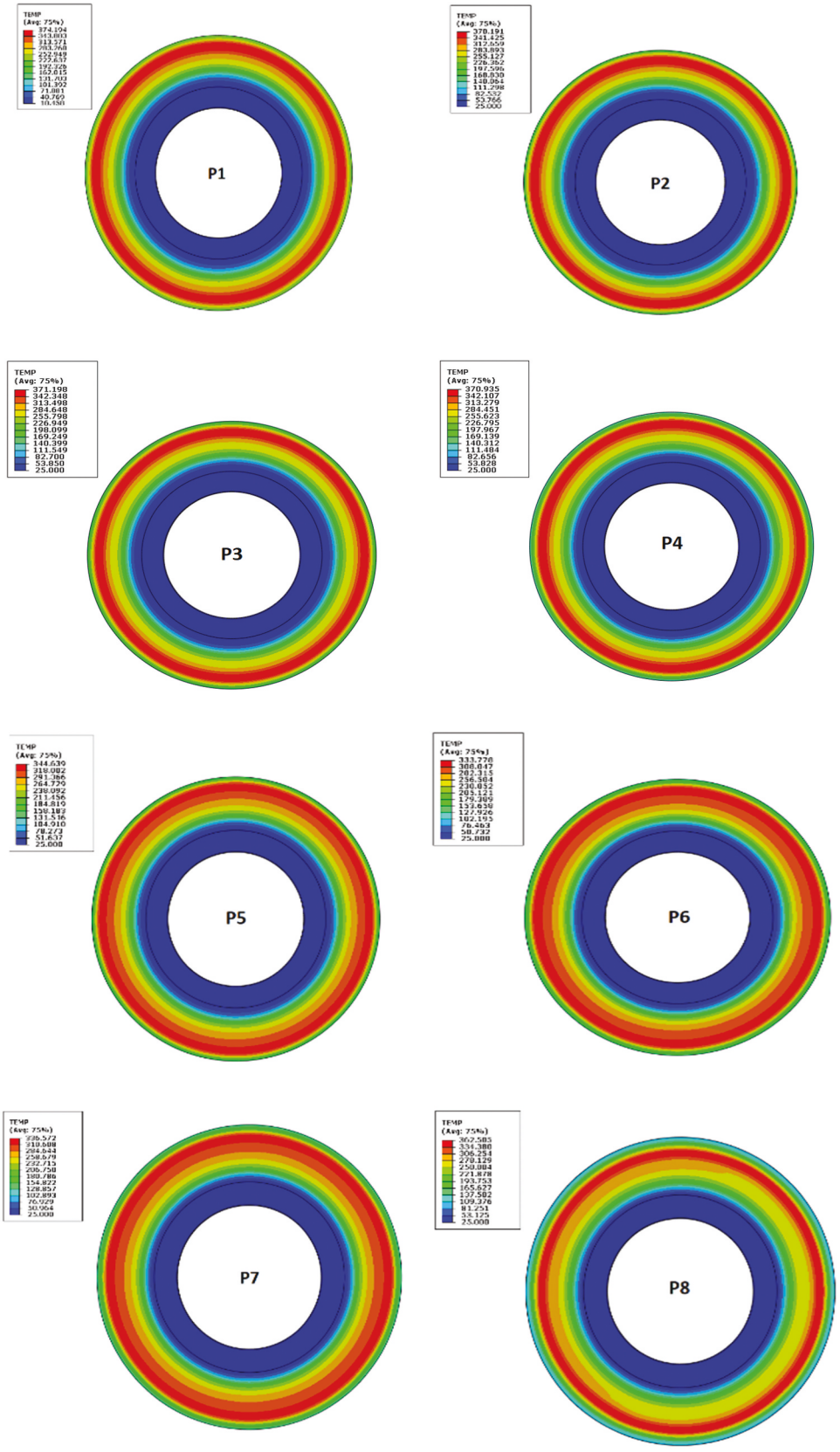

Figure 11. Variation of temperature field on disc for different positions of the pads.

positions. Nonetheless, at P8, a highly concentrated red zone and an irregular temperature field distribution appeared on some regions of the disc. Generally, it was observed that the more spread and uniform the red zones, the lower the peak temperature exhibited.

In addition, the variation of maximum temperature in each disc at the various pad positions with time was observed as shown in (Figure 12). It was observed that the heat generation in the disc labelled P1, P2, P3, and P4 rises faster at the initial stage of the braking process

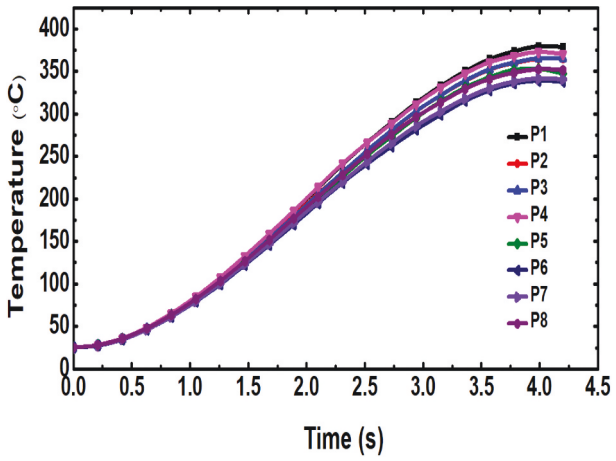

Figure 12. Variation of maximum temperature with time at different pad positions on the disc.

to maximum values of 374.19°C, 370.19°C, 371.20°C,

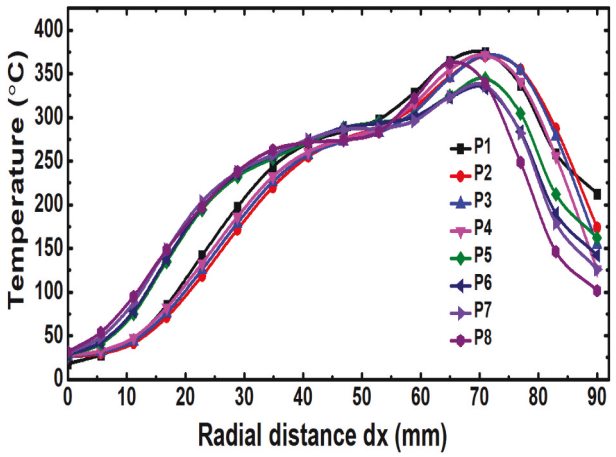

Figure 13. Distribution of temperature along the radial of the disc for different pad positions.

and 370.94°C, respectively, compared to P5, P6, and P7.

Besides, the disc labelled P6 exhibited the lowest maximum temperature with time compared to all the other discs during the simulation process, this makes it more appropriate for the reference vehicle in terms of temperature distribution. Moreover, along the radial of the friction ring section of the discs, as shown in (Figure 13), the radial temperature field distribution for P1, P2, P3, and P4 exhibited similar temperature distribution profile while the disc labelled P5, P6, P7, and P8 also assumed the same profile pattern but different from the first four positions mentioned earlier. Nevertheless, a significant sharp rise in temperatures was observed at a radial distance ranging from dx = 65 mm to dx = 80 mm for P1, P2, P3 P4, and P8. The effect of this behaviour on thermal buckling during braking is investigated in Section 4.3.

4.3. Effects of resulting radial temperature distribution on thermal buckling

In this section, we determined the resulting critical thermal buckling temperatures resulting from the contact geometry analysis in sections 4.1 and 4.2. A linear perturbation procedure was used based on the eigenvalue approach because, even if the disc has nonlinearity in terms of geometry, material, and so on, a general eigenvalue buckling mode is sufficient to render useful information on the deformation mode. ABAQUS script was utilised to compute the thermal buckling mode of the rotor for the radial temperature distribution resulting from varying the pad cover angle and pad positions on the disc. The pre-loaded temperature fields (Figures 10 & 13) of the friction ring section of the rotor were expressed in polynomial functions of the sixth-order and applied in the linear perturbation analysis. The solution gives the deformation modes and the force multipliers $\lambda_i$for the temperature loads $f_i$defined. We utilised the force multipliers also referred to as the eigenvalues to compute the corresponding buckling temperatures for each analysis. Thermal buckling occurs when the maximum braking temperature or the applied temperature load exceeds the computed critical buckling temperature and the rotor can be said to have undergone deformation or buckling. The first three deformation modes of the disc by varying the pad cover angle (θp = 20°) and the pad position at $R_p = R_d$are showed in (Figures 13 and 14). Mapping the deformation modes in (Figures 14 to 15) show that the deformation modes are similar for the two scenarios considered. This may be due to the close-range temperature distribution observed in both contact geometry analyses. Nonetheless, their resulting eigenvalues or force multipliers were different. The corresponding eigenvalues for mode 1, mode 2 and mode 3, by varying the cover pad angles (θp = 20°) were found to be 1.007, 1.073 and 1.104, respectively, while the corresponding eigenvalues for the modes by varying the pad position at $R_p = R_d$were 1.154, 1.227 and 1.270 for modes 1, 2 and 3, respectively. The critical buckling temperatures f_{cr}were obtained by finding the product of the applied maximum temperature load and its corresponding eigenvalue or buckling load multiplier, that is, $f_{cr} = \lambda_i f$.

(Tables 3 and 4) show the critical thermal buckling temperatures for the first six modes when the angles and positions of the pads were varied, respectively. From (Table 3), it can be deduced that the influence of pad cover angles on the critical buckling temperature of the disc is less significantly compared to varying the pad positions as seen in (Table 4). This could be attributed to the small and more uniform temperature field distribution associated with varying the pad cover angles than varying the pad positions. As

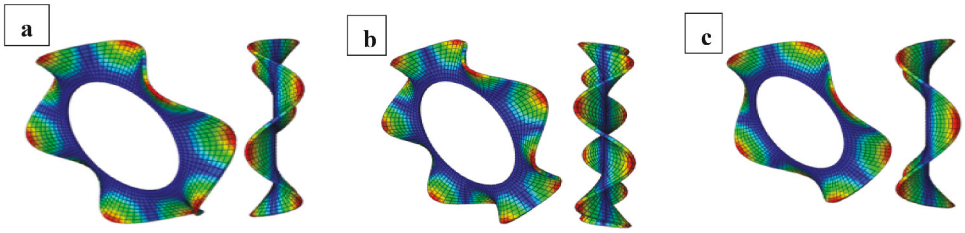

Figure 14. Deformation modes for thermal Buckling at θp = 20°a) First-Order buckling mode b) Second-Order buckling mode c) third-Order buckling mode.

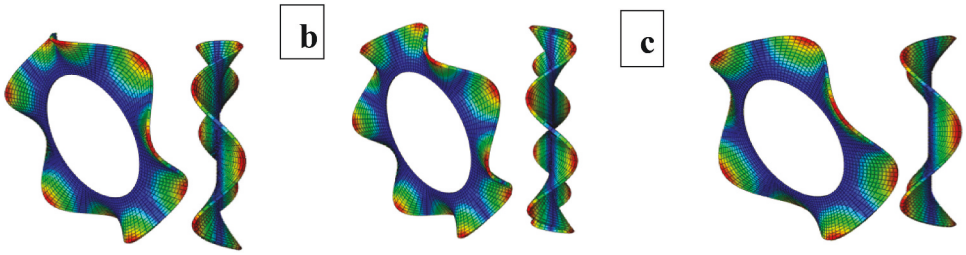

Figure 15. Deformation modes for thermal Buckling at $R_p = R_d$**a)** First Order buckling mode **b)**Second-Order buckling mode **c)** third Order buckling mode.

Table 3. Buckling temperatures on the disc for various pad cover angles.

Mode	Buckling Temperature along the radial							
	20	30	40	50	60	70	80	90
1	357.9	356.2	374.9	389.9	410.8	467.1	437.6	457.5
2	381.3	379.4	399.3	415.2	437.4	496.8	465.8	486.6
3	392.3	390.4	411.1	427.8	451.0	514.3	480.7	503.3
4	434.7	432.6	455.3	473.4	498.7	566.1	531.1	554.6
5	508.6	506.2	532.9	554.2	583.9	662.8	621.9	649.5
6	−583.7	−581.2	−608.9	−631.2	−661.3	−738.0	−702.0	−725.8

a result, the critical buckling temperatures were found to be higher than the braking temperature for all varied angles (θ_p). Hence, no buckling occurred during braking by varying the cover angles. Meanwhile, some of the critical buckling values exhibited were close to the onset of thermal buckling. For example, considering the disc with pad cover angle of 20°, the difference in the critical temperature (357.9°C) and braking temperature (355.4°) was quite close. This could result in buckling of the disc during multiple braking of the vehicle.

Conversely, when the pad positions were varied at these positions: $r_p = 172.1 < r < R_p = 236$, $r_p = 170.8 < r < R_p = 235$, $r_p = 168 < r < R_p = 233$, $r_p = 166.6 < r < R_p = 232$ and $r_p = 165.2 < r < R_p = 231$, the corresponding braking temperatures on the various discs exceeded the critical buckling temperature. This is because the temperature difference between the inner and outer radius of the disc is significant or highly non-uniform. For example, considering the disc with pad positioned at $r_p = 172.13\ mm < r < R_p = 236\ mm$, the first-order eigenvalue was 0.817. The corresponding buckling temperature (302.7°C) was smaller than the maximum braking temperature (370.1°C), leading to deformation. It is important to note that the negative temperatures associated with the sixth mode for the pad cover angles and certain positions of the pads indicate that the corresponding eigenvalues were negative and that deformation will occur when the applied temperature load direction is reversed.

Besides, from the results in (Table 4), it can be deduced that the pad positions on the disc have a significant effect on the thermal buckling of the rotor during braking of the reference vehicle even by considering the same moment of friction because of the highly non-linear temperature distribution exhibited.

5. Conclusion

The work presents a study on the contact geometry of an in-wheeled disc brake during single braking at full vehicle load with an initial velocity of 30 km/h on a flat road without steering. The effects of the cover angle of the pad and its position on the disc brake during the braking period are investigated. Further, the effect of the resulting radial temperature distribution on

Table 4. Buckling temperatures on the disc for various pad positions on the disc.

Mode	Buckling Temperature along the radial							
	$R_p = R_d$	$r_p = 172.13 < r < R_p = 236$	$r_p = 170.76 < r < R_p = 235$	$r_p = 169.4 < r < R_p = 234$	$r_p = 168 < r < R_p = 233$	$r_p = 166.6 < r < R_p = 232$	$r_p = 165.2 < r < R_p = 231$	$r_p = 163.8 < r < R_p = 230$
1	431.7	302.7	334.1	574.8	341.5	291.5	254.1	518.0
2	459.2	322.6	356.1	608.5	363.5	310.5	270.6	548.9
3	474.9	331.0	365.7	637.3	374.6	319.3	277.9	573.7
4	523.4	367.5	405.8	691.2	414.3	353.6	307.9	623.9
5	612.9	429.3	474.6	807.1	484.7	413.3	359.3	729.0
6	−687.5	504.9	−552.7	−875.9	−556.6	−482.5	422.0	−795.7

thermal buckling for the investigated contact geometry of the disc during braking is a second consideration in the work. The following conclusions are drawn:

(1) For design purposes, even if the same friction work is maintained for different pad sizes or cover angle in a brake system such as the in-wheel mounted brake discussed in this work, the resulting temperature fields are significantly different. The maximum temperature on the disc is inversely proportional to the pad size or cover angle even for the same friction work. Therefore, an optimum choice of pad cover angle is important in design to prevent the early onset of thermal buckling and thermoelastic instability.
(2) The sensitivity of pad positions on disc brake to thermal buckling and thermomechanical instability is significant. This work revealed that even maintaining the same friction work for different pad locations on the disc during braking has a significant influence on the temperature field distribution. Depending on the position of the pad, the peak temperatures and temperature field distribution can vary greatly. The temperature distribution for disc P1 where $R_p = R_d$ and P8 where $r_p = (163.81 < r < R_p = 230)$ was found to be inappropriate for the in-wheeled brake system in terms of temperature field distribution. However, at these positions and also at $r_p = 169.4 < r < R_p = 234$ and $r_p = 165.2 < r < R_p = 231$, thermal buckling did not occur during braking. In general, the position of pads on the disc surface has a significant effect on the thermal buckling of the disc during braking.

Acknowledgments

Support for this work, provided by the National Science Foundation under Contract (No. 1928876), is gratefully acknowledged.

Disclosure statement

No potential conflict of interest was reported by the author(s).

Funding

This work was supported by the National Science Foundation [No. 1928876].

Notes on contributors

Kingsford Koranteng is currently a PhD student and graduate research assistant in the Department of Mechanical & Materials Engineering at University of Denver, U.S.A. His current research interest is mainly in Thermal-mechanical instability in sliding systems such as automobile brakes and clutches. He received his bachelor's degree in Agricultural Engineering from University of Ghana in 2016 and his master's degree in Mechanical Engineering from Beijing Institute of Technology in 2019.

Joseph-shaahu Shaahu is currently a Ph.D. candidate and graduate research assistant in Mechanical Engineering at the University of Denver. He obtained his BSc from Purdue University and his MSc from University of Denver with a focus in Solid Mechanics and Computational Analysis. His current research interests include anisotropic metal free friction materials and thermal-mechanical instabilities.

Dr. Yun-Bo Yi is a Professor in the Department of Mechanical and Materials Engineering with a joint appointment in the Department of Electrical and Computer Engineering at the University of Denver, U.S.A. He authored/coauthored nearly 80 journal and conference publications. His research interests include stabilities in sliding systems, energy dissipation in MEMS sensors, and computational modeling of multiscale heterogeneous materials. He teaches undergraduate and graduate courses in Engineering Mechanics, Machine Design, Mechanics of Materials, Numerical Methods and Elasticity. He is the author of Hotspotter, an engineering analysis program to determine the susceptibility of disc brakes, clutches and other frictionally sliding systems to thermoelastic instability. He is currently an Associate Editor of ASME Journal of Tribology.

ORCID

Kingsford Koranteng http://orcid.org/0000-0002-5369-4275
Yun-Bo Yi http://orcid.org/0000-0001-9936-854X

Data Availability

All data generated or analysed during this study are included in this published article (and its supplementary information files).

Nomenclature

a_d	Contact on the disc, (m^2)
A_s	Contact surface area (m^2)
a_j	Deceleration of the vehicle, (m/s^2)
D	Disc diameter,(m)
F_z	Vertical force on the wheel, (N)
P_d	Decelerating power (W)
$q(r,t)$	Heat flux (W)
I	Mass moment of inertia for all rotating parts $(200kgm^2)$
p	Contact pressure (MPa)
R_w	Wheel radius, (m)
T_a	Ambient/Initial temperature, $(^\circ C)$
T_{max}	Maximum temperature, $(^\circ C)$
T	Temperature
h	Heat coefficient $(W/m^2/^\circ C)$
Z	Axial position

(*Continued*)

a_d	Contact on the disc, (m^2)
A_s	Contact surface area (m^2)
a_j	Deceleration of the vehicle, (m/s^2)
D	Disc diameter,(m)
F_z	Vertical force on the wheel, (N)
P_d	Decelerating power (W)
$q(r,t)$	Heat flux (W)
I	Mass moment of inertia for all rotating parts $(200kgm^2)$
p	Contact pressure (MPa)
R_w	Wheel radius, (m)
T_a	Ambient/Initial temperature, $(^\circ C)$
T_{max}	Maximum temperature, $(^\circ C)$
T	Temperature
h	Heat coefficient $(W/m^2/^\circ C)$
Z	Axial position
r	radius, (m)
$(r,,0,t)$	Cylindrical-coordinate system
v	velocity (m/s)
t	Time (s)
Q_{in}	Amount of heat generated
Q_{out}	Amount of heat dissipated
ρ	Density (kg/m^3)
	Angular velocity(rad/s)
a_t	Angular acceleration (rad/s^2)
v	Kinematic viscosity of air (m^2/s)
α	Thermal diffusivity (m^2/s)
K	Thermal conductivity $(W/m^{2^\circ}C)$
δ_d	Thickness of the disc (m)
γ	heat partition coefficient
Subscript	
$p,d,$ s	Pad, disc, surface
R,L	Right wheel, Left wheel
o,i,f	Initial, Initial, final
a	air

References

Adamowicz, A., and P. Grześ. 2012. "Convective Cooling of a Disc Brake during Single Braking." *acta mechanica et automatica* 6.

Belhocine, A., and M. Bouchetara. 2012. "Thermal Analysis of a Solid Brake Disc." *Applied Thermal Engineering* 32: 59–67. doi:10.1016/j.applthermaleng.2011.08.029.

Chen, Z., Y.-B. Yi, K. Bao, and J. Zhao. 2019. "Numerical Analysis of the Coupling between Frictionally Excited Thermoelastic Instability and Thermal Buckling in Automotive Clutches, Proceedings of the Institution of Mechanical Engineers, Part J." *Journal of Engineering Tribology* 233: 178–187.

Chen, Z., Y.-B. Yi, and J. Zhao. 2016. "Fourier Finite Element Model for Prediction of Thermal Buckling in Disc Clutches and Brakes." *Journal of Thermal Stresses* 39 (10): 1241–1251. doi:10.1080/01495739.2016.1215728.

Choi, J.-H., and I. Lee. 2004. "Finite Element Analysis of Transient Thermoelastic Behaviors in Disk Brakes." *Wear* 257 (1–2): 47–58. doi:10.1016/j.wear.2003.07.008.

Ghadimi, B., R. Sajedi, and F. Kowsary. 2013. "3D Investigation of Thermal Stresses in a Locomotive Ventilated Brake Disc Based on a Conjugate Thermo-fluid Coupling Boundary Conditions." *International Communications in Heat and Mass Transfer* 49: 104–109. doi:10.1016/j.icheatmasstransfer.2013.10.009.

Grze, P. 2011. "Partition of Heat in 2d Finite Element Model of a Disc Brake." *acta mechanica et automatica* 7.vol.5 no.2

Grześ, P. 2014. "Numerical Analysis of Temperature Field in a Disc Brake at Different Cover Angle of the Pad." *Acta Mechanica et Automatica* 8 (4): 185–188. doi:10.2478/ama-2014-0033.

Grzes, P., W. Oliferuk, A. Adamowicz, K. Kochanowski, P. Wasilewski, and A.A. Yevtushenko. 2016. "The Numerical–experimental Scheme for the Analysis of Temperature Field in a Pad-disc Braking System of a Railway Vehicle at Single Braking." *International Communications in Heat and Mass Transfer* 75: 1–6. doi:10.1016/j.icheatmasstransfer.2016.03.017.

He, L., and T.C. Ovaert. 2008. "Heat Partitioning Coefficient Calculations for Sliding Contacts with Friction." *Tribology Transactions* 51 (1): 12–18. doi:10.1080/10402000701739248.

Hwang, P., X. Wu, and Y. Jeon. 2008. "Repeated Brake Temperature Analysis of Ventilated Brake Disc on the Downhill Road."

Karan Dhir, D. 2018. "Thermo-mechanical Performance of Automotive Disc Brakes." *Materials Today: Proceedings* 5: 1864–1871.

Koranteng, K., J.-S. Shaahu, M. Chengnan, H. Li, and Y.-B. Yi. 2020. "The Performance of Cu-based Friction Material in Dry Clutch Engagement." *Proceedings of the Institution of Mechanical Engineers, Part J: Journal of Engineering Tribology* 135065012094428. 235(6): 1114-1123

Shaahu, J., K. Koranteng, and Y.-B. Yi. 2020. *A Coupling Analysis of Thermal Buckling and Vibration in Disc Brakes*. https://www.sae.org/publications/technical-papers/content/2020-01-1606/

Talati, F., and S. Jalalifar. 2009. "Analysis of Heat Conduction in a Disk Brake System." *Heat and Mass Transfer* 45 (8): 1047–1059. doi:10.1007/s00231-009-0476-y.

Tsai, H.-L., H.-G. Teo, C. Gau, S.T. Jeng, C.C. Lee, S.W. Lin, and S.C. Lin. 2007. TRANSIENT THERMAL ANALYSIS OF A DISK BRAKE SYSTEM. In *Proceedings of the 14th National Computational Fluid Dynamics Conference,* 27–29. New Taipei City, Taiwan.

Vescovini, R., and L. Dozio. 2018. "Thermal Buckling Behaviour of Thin and Thick Variable-Stiffness Panels." *Journal of Composites Science* 2 (4): 58. doi:10.3390/jcs2040058.

Wang, G., and R. Fu. 2013. "Impact of Brake Pad Structure on Temperature and Stress Fields of Brake Disc." *Advances in Materials Science and Engineering* 2013: 1–9.

Yevtushenko, A., and P. Grzes. 2011. "Finite Element Analysis of Heat Partition in a Pad/Disc Brake System." *Numerical Heat Transfer, Part A: Applications* 59 (7): 521–542. doi:10.1080/10407782.2011.561098.

Yi, Y.-B., J.-S. Shaahu, and Z. Chen. 2018. "Instabilities Induced by Thermal-Mechanical Couplings in Clutch and Brake Discs."